Solidification Modeling of Complex-Shaped

Single Crystal Turbine Airfoils

K.O. Yu*, J.A. Oti*, M. Robinson* and R.G. Carlson**

* PCC Airfoils, Inc., Beachwood, Ohio
** GE Aircraft Engines, Cincinnati, Ohio

Abstract

Single crystal turbine airfoils casting integrity depends on structures as well as inherent defects. PCC Airfoils, in conjunction with the Air Force MANTECH program and GE Aircraft Engines (GEAE), correlated the solidification conditions to the microstructures and defects of single crystal castings. The approach combined finite-element thermal analysis and experimental results. Simple-shaped cylinders were first cast and modeled to establish a defects prediction map. Solidification conditions of complex-shaped airfoils were then modeled, to predict the evolution of casting microstructures as well as the occurrence of casting defects by using the pre-established defects map. Comparison of model predictions to experimental inspection results show that finite-element modeling is an effective tool for understanding the solidification sequence and predicting the microstructure, defects and chemistry variation of investment cast, complex-shaped, single crystal turbine airfoils.

Superalloys 1992
Edited by S.D. Antolovich, R.W. Stusrud, R.A. MacKay,
D.L. Anton, T. Khan, R.D. Kissinger, D.L. Klarstrom
The Minerals, Metals & Materials Society, 1992

Introduction

Although single crystal castings promise higher performing products in jet engines, they present foundry manufacturing problems. For a complex single crystal blade or vane design, optimizing all casting variables is almost impossible with state-of-the-art, casting methods. Finite-element thermal modeling offers the capability of simulating casting solidification and understanding the solidification sequence. Efforts were undertaken in the Air Force/GEAE MANTECH program and at PCC Airfoils, to develop a software (Single Crystal Modeler, SCM) and establish a methodology to simulate the solidification of single crystal castings. The SCM takes geometrical data, constructs a 3-D model of the part, adds gating and mold material, enmeshes the mold-metal system, performs solidification simulation, displays the results graphically, and permits variations by the casting engineer so that the best production process can be selected.

The approach combined finite-element thermal analysis and experimental results. Simple-shaped cylinders were first cast and modeled to establish a defects prediction map. The solidification conditions of two complex shaped airfoils, high pressure turbine vane (HPTV) and low pressure turbine blade (LPTB), were then modeled to predict the casting microstructures and defects, by using the pre-established defects map. The model predicted results were validated by comparing them to experimental inspection results. To further validate the applicabilities of the modeling methodology and defects map established in the MANTECH program, another airfoil (high pressure turbine blade, HPTB) was modeled by using a commercial finite-element code ProCAST for a GEAE internally supported program.

Modeling results and the method for developing a defects map from simple shaped cylinders have been reported elsewhere[1]. The purpose of this paper is to present results from the modeling of complex-shaped airfoils.

Approach

The approach combines finite-element thermal analysis and experimental results. Cylinders were first cast and modeled to establish a defects prediction map[1]. Several molds of complex-shaped airfoils were then cast and the solidification conditions of those airfoils were modeled, to predict the evolution of casting microstructures and the occurrence of casting defects by using the pre-established defects map. Finally, these model predictions were compared to casting inspection results.

Experimental Procedure

Clusters (Figure 1) of three different complex-shaped airfoils (HPTV, LPTB and HPTB) were cast at specified furnace temperature and withdrawal speeds. Thermocouples were placed in the mold, metal and core to record the temperature as a function of time at specified locations. After shake-out of the mold, castings were inspected by grain etching, FPI (fluorescent penetrant inspection), X-ray and Laue' X-ray for grain defects, porosities and primary dendrite directions. Numerous specimens were cut from as-cast castings to measure the primary and secondary dendrite arm spacing (PDAS and SDAS). For one particular airfoil configuration (HPTB), samples were taken from root and tip regions for Y, Al, Si and Zr analysis.

Finite-Element Modeling

Details of the procedure for finite-element modeling of single crystal castings have been described in Reference 1, and interested readers should

reference that paper. In general, metal and core geometries can be generated from any commercial software such as PATRAN, IDEAS and ANSYS. The mesh for the ceramic mold around the metal was semi-automatically generated through the use of EXTRUDE program in IDEAS for HPTV and LPTB models. A PCC Airfoils proprietary software was used to generate mold for the HPTB model. The finite-element solutions were obtained by TOPAZ/ SDRC for HPTV and LPTB and by ProCAST for HPTB. Modeling results included isotherms, isochrons (time to reach the specified temperatures), temperature gradients G, solidification rates R, combinations of G and R, cooling rates, local solidification times (LST) and cooling curves.

The finite-element model of HPTV is shown in Figure 2. Figure 3 shows the cluster configurations of HPTV and LPTB. It can be seen that the part, the furnace, and the copper chill are all incorporated into these finite-element models. The initial temperature conditions of the metal, core and mold were assigned based on the thermocouple readings of those experimental castings. The boundary conditions of the furnace wall temperature were also applied based on thermocouple data.

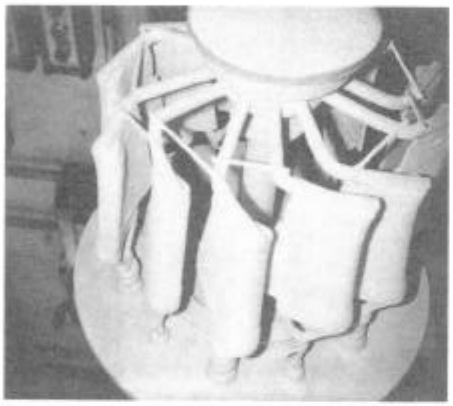

FIGURE 1. Experimental Cluster of HPTV.

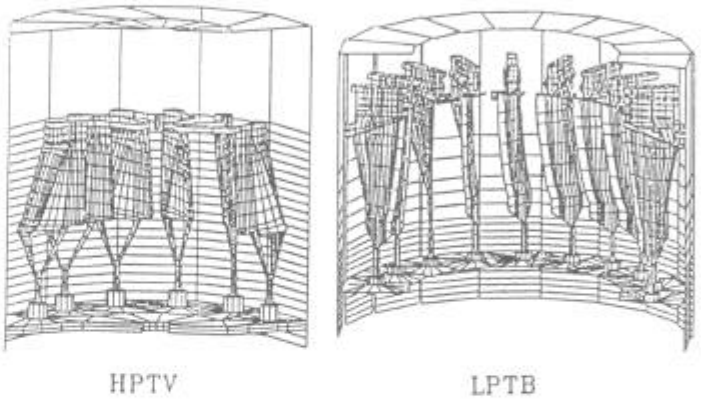

FIGURE 3. Cluster Configuration of HPTV and LPTB Models.

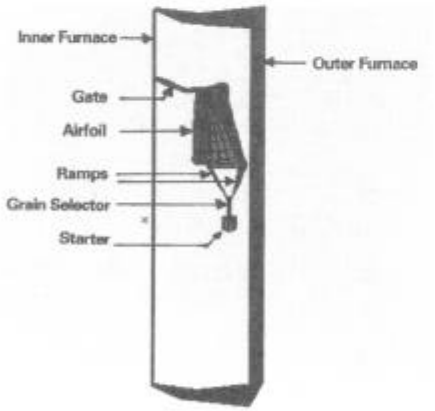

FIGURE 2. Finite-Element Model of HPTV.

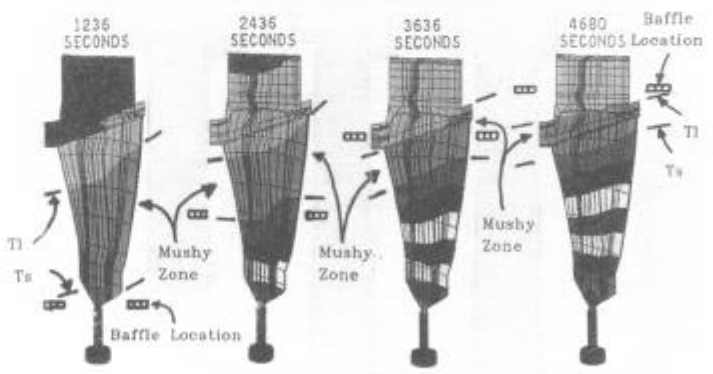

FIGURE 4. Model Calculated Isotherms of LPTB at Various Withdrawal Times.

The calculated isotherms of LPTB at various withdrawal times are shown in Figure 4. Figure 5 shows the calculated cooling curves of LPTB. Thermocouple data at the location of Node 2689 is also shown.

Results and Discussion

Based on the pre-established defects map, microstructures and defects of the complex-shaped airfoils are predicted and compared with casting

inspection results. The change of Y, Al, Si and Zr contents of HPTB is also correlated with model calculated solidification conditions.

Dendrite Arm Spacing

For dendritic solidification, DAS is the most convenient parameter for representing the degree of microsegregation of castings. The fineness[1,2] of DAS is directly related to LST or average cooling rate during solidification. As heat is extracted faster from castings (i.e., shorter LST and higher average cooling rate), the size of the resulted DAS and the degree of the associated microsegregation are also smaller. The DAS predictor was established by correlating measured DAS values from experimental castings to model calculated LST. Figures 6 and 7 show this correlation for PDAS and SDAS. Based on these results, Figure 8 presents a comparison of LPTB model predicted DAS values versus measured DAS values.

Grain Defects

Numerous grain defects were found in experimental castings, including high/low angle boundaries (HAB and LAB), bigrains, equiaxed grains and freckles. The formation of these grain defects are related to casting solidification conditions. Misoriented dendrite (MOD) is not a grain defect but its formation is clearly related to the contour of the solidification front, and is also discussed in this section. On the other hand, sliver is a type of grain defect which is primarily related to metal-ceramic reaction and is discussed in that section.

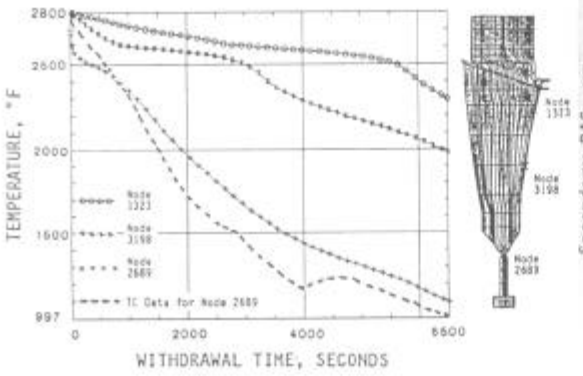

FIGURE 5. Model Calculated and Experimentally Recorded Cooling Curves of LPTB.

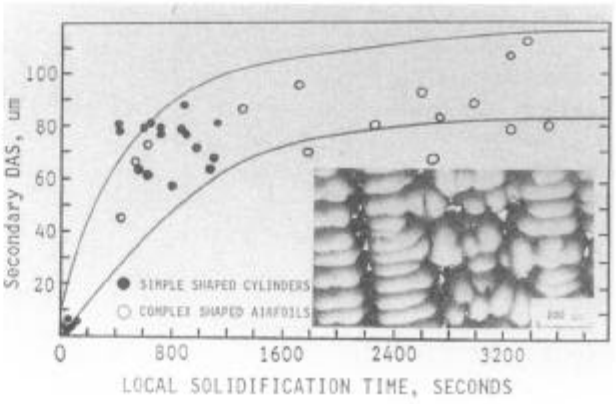

FIGURE 7. Measured SDAS as a Function of Model Calculated LST.

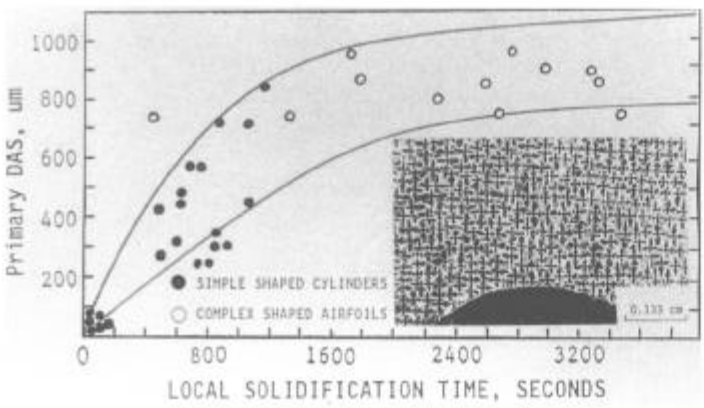

FIGURE 6. Measured PDAS as a Function of Model Calculated LST.

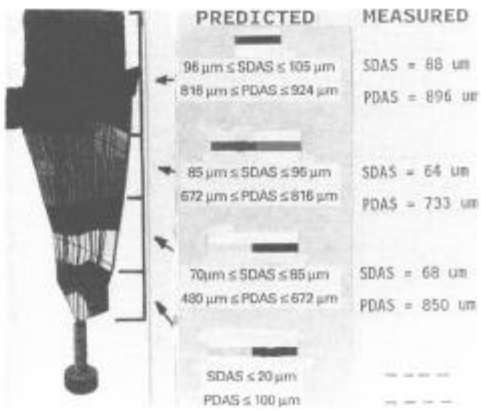

FIGURE 8. Comparison of Predicted and Measured DAS for LPTB.

High/Low Angle Boundaries and Bigrains. Grain defects that are functions of the contour and orientation of the solidification front include HAB, LAB, bigrains and multigrains. Dendrites grow opposite the direction of the heat flow, perpendicular to the mushy zone contour. When dendrites of different orientation meet, HAB or LAB may form depending on the magnitude of the angle between dendrites. In Figure 9, the trailing edge of the HPTV cools much faster than the leading edge side. Consequently, the mushy zone forms an "L" shaped contour, and a grain boundary is expected to form at the location where dendrites with different growth directions meet. In the casting, the dendrite growth direction is consistent with the model prediction. The two dendritic orientations meet to form a grain boundary. Because this is a single crystal alloy, there are no grain boundary strengthening constituents, and a crack forms along the grain boundary.

Sometimes a second solidification front is also present in the casting. Usually this second solidification front is located near the trailing edge of the casting because it is thin there and, hence, it tends to cool faster than the rest of the casting. As a result, two grains with different crystallographic orientations form. This type of defect is called bigrains. If more than two grains are present simultaneously in the casting, it is called multigrains.

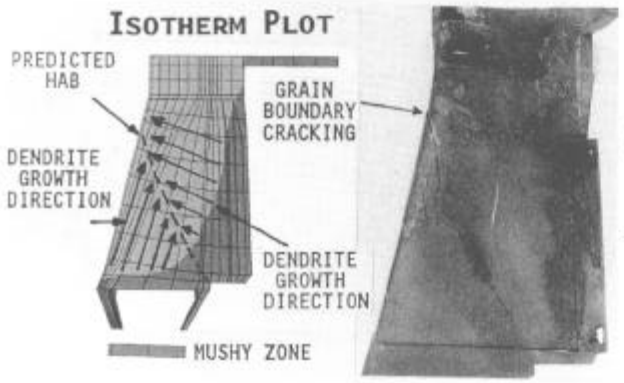

FIGURE 9. Comparison of Model Predicted and Experimentally Inspected HAB for HPTV.

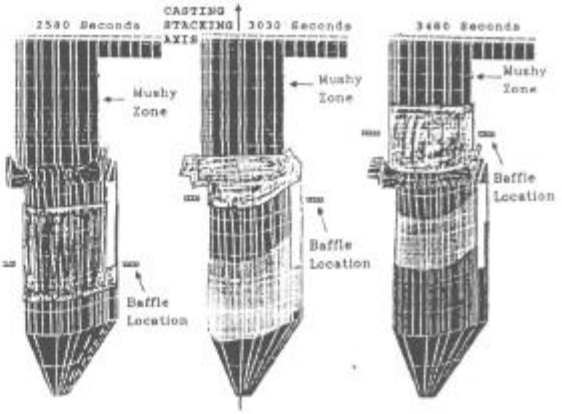

FIGURE 10. Calculated Isotherms at Various Withdrawal Times for Lot 15 of HPTB.

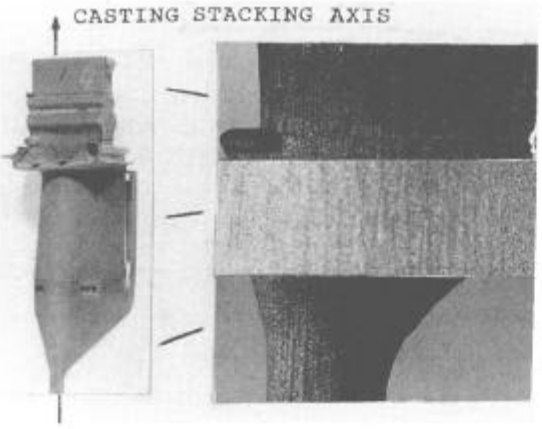

FIGURE 11. Primary Dendrite Growth Direction of a HPTB Casting of Lot 15.

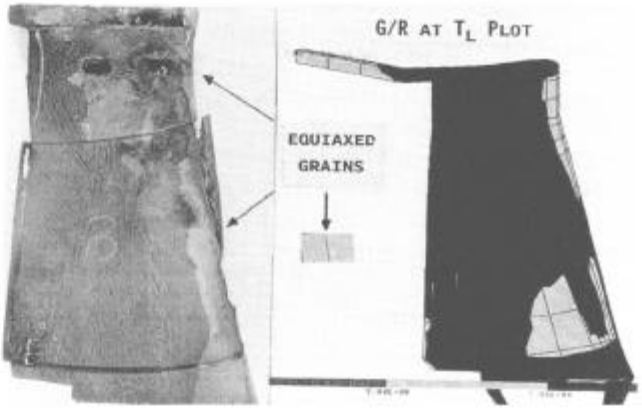

FIGURE 12. Comparison of Predicted and Inspected Equiaxed Grains for HPTV.

Misoriented Dendrite Direction. Since the dendrite growth direction is directly opposite to the heat flow direction and perpendicular to the mushy zone contour, the mushy zone contour is also used to predict the MOD.

Laue' back reflection x-ray technique is used to determine the deviation of the primary dendrite growth direction from the stacking axis of the airfoil. When deviations are beyond a specified value, castings are rejectable. In Figure 9 the mushy zone contour indicates that the angle between the dendrite growth direction and the stacking axis of the HPTV is high and thus the castings have a high tendency to be rejected by Laue' inspection. Laue' results of these castings show a high casting rejection rate, which is consistent with model predictions. Figure 10 shows that the calculated isotherm contours of HPTB are always perpendicular to the casting stacking axis, indicating the primary dendrite growth direction should be parallel to the casting stacking axis. This prediction is consistent with the results from microstructure evaluation (Figure 11). Laue' results also show that all castings pass the inspection.

Equiaxed Grains. During solidification, the solidification front morphology is controlled by the combination of the temperature gradient G in the liquid phase just ahead of the advancing interface, and by the interface velocity or solidification rate R[3,4]. In this study, equiaxed grains are predicted by the G/R at the liquidus temperature. The higher the G/R value, the lower the equiaxed grains formation tendency. Figure 12 compares a G/R plot with a grain photograph of an HPTV casting. The low G/R patches on the leading edge of the model (which indicates equiaxed grains will form) are consistent with the equiaxed grains found on the casting.

Freckles. Interdendritic fluid flow in the mushy zone during solidification is responsible for freckle-type defects[5-8]. Gell and Duhl[9] showed that the formation of this interdendritic fluid flow is controlled by the casting average cooling rate during solidification. Based on previously established freckle formation criterion[1], model predictions indicate that no freckles should be present in these castings. This conclusion is consistent with casting inspection results.

Shrink Defects

There are two specific types of shrink; macroshrink and microporosity. Macroshrink is controlled by bulk heat transfer conditions, whereas microporosity is related to the feeding conditions in the mushy zone.

Macroshrink. In the casting, if there is an isolated region which is last to solidify, then macroshrink forms in that region[10]. Equiaxed castings usually have a higher tendency to form macroshrink than directionally solidified and single crystal castings do. The formation of macroshrink is predicted by the contour of the solidus isochron. An isochron is a contour plot which illustrates regions of constant time for castings to cool to a specified temperature. In the solidus isochron plot, an isolated spot with a higher time to reach solidus temperature means metal in that spot is the last to solidify and macroshrink is expected to form in that spot. There are no isolations in Figure 13 which could create macroshrink, and this prediction is verified by casting inspection results.

Microporosity. Microporosity forms near the end of solidification in the interdendritic regions when capillary feeding becomes insufficient[11]. Thus the propensity of the microporosity formation is related to the casting feeding ability during the last stage of solidification, which is controlled by the G/R at the solidus temperature[12,13]. The lower the G/R at solidus value, the higher the tendency that microporosity forms. Microporosity can show up on or beneath the surface of the casting. Based on previously established microporosity formation criterion[1], modeling results indicate very low tendency for surface microporosity formation in

the HPTV castings, and verifies this with FPI inspection results. Figure 14 compares the internal microporosity seen at x-ray on the HPTV with the model predicted results. The model prediction indicates that all the castings should have internal microporosity. This prediction is not completely consistent with casting inspection results. However, the model predicted relative trends (i.e., a bigger light color area indicates a higher tendency) to form microporosity in castings of these four molds are very consistent with inspection results.

Effects of Metal-Ceramic Reaction

Chemical reaction between ceramics (mold and core) and active elements such as Y in the metal results in a decrease of metal Y content and increase of metal inclusion content. The later effect then increases the tendency for the formation of slivers.

Active Elements Control. For each mold of HPTB, samples were taken from root and tip regions of castings for Y, Al, Si and Zr analysis. Results are shown in Table 1. From the table it can be seen that:

1. For all molds, the Y content in the tip region is always higher than that of the root region, whereas tip Si content is always lower than the root Si content. This indicates that the primary reason for Y loss is due to the reaction between Y and SiO_2. There seems no clear correlation between Al and Zr contents and Y content.

2. Lots 15 and 16 have a 40% lower initial Y content than Lot 5, but the casting Y content for these three molds is practically the same. If we define the ratio of the casting final Y content to its initial Y content as Y retention efficiency, Table 1 indicates that Lots 15 and 16 have a much higher Y retention efficiency than Lot 5.

3. Casting Y content of Lots 11-13 is significantly higher than that of Lot 5 (all four molds have the same casting condition). Although Lots 11-13 have a 10% higher initial Y content than Lot 5, the magnitude of the difference of the resultant casting Y content is still a surprise.

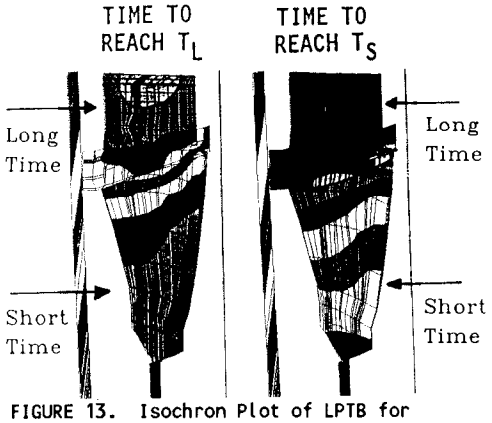

FIGURE 13. Isochron Plot of LPTB for Prediction of Macroshrink.

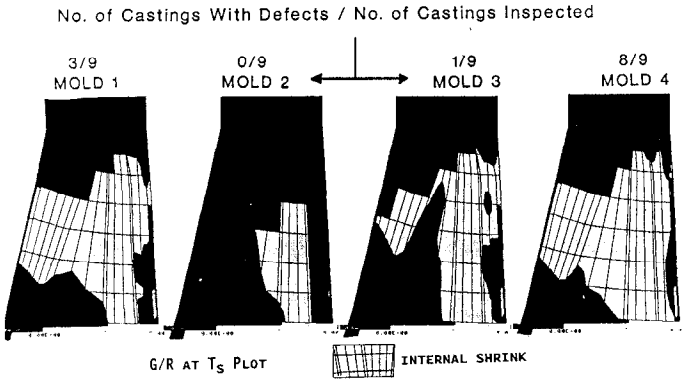

FIGURE 14. Comparison of Model Predicted and X-Ray Inspected Internal Shrink for HPTV.

Assuming a constant initial Y content, the amount of Y loss during casting depends on the chemical reaction rate between molten metal and surrounding ceramics. Three most important factors controlling the kinetics of this metal-ceramic reaction are casting geometry (surface to volume ratio), reaction temperature and contact time. For the data shown in Table 1, casting geometry and reaction temperature (all six molds are cast at the same preheat and pour temperature) are practically constant, and only

metal-ceramic contact time is the important controlling factor. A longer contact time results in a bigger Y loss and a lower Y retention efficiency.

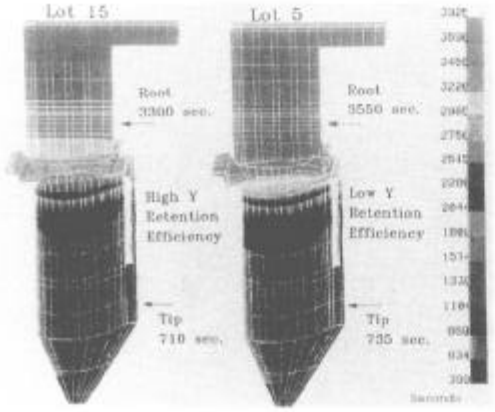

FIGURE 15. Isochron Plot for Lot 5 and 15 of HPTB.

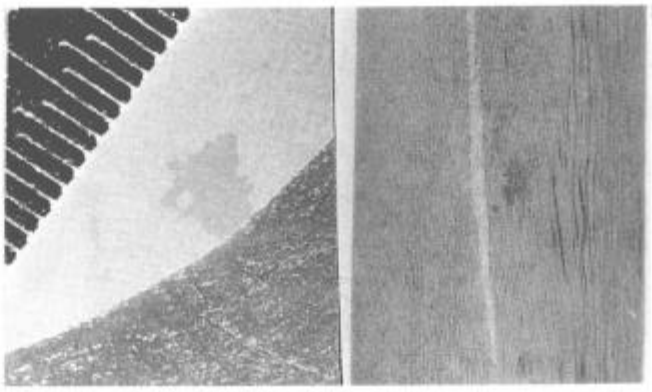

FIGURE 16. Transverse and Longitudinal View of a Sliver

Figure 15 shows the isochron plot for castings of Lots 5 and 15. In this figure, the isochron is the time for the metal to cool from pour temperature to the metal solidus temperature. Thus, the isochron shown in Figure 15 represents metal-ceramic contact time before metal is completely solidified. From the figure it can be seen that the isochron of the castings of Lot 15 are lower than that of Lot 5, indicating castings of Lot 15 should have a higher Y retention efficiency than that of Lot 5. A similar conclusion was reached for Lot 16. These model predictions are consistent with inspection results shown in Table 1.

TABLE 1. Y content of HPTB castings with various casting conditions and initial Y content.

	Lot 5		Lots 11/12/13 *		Lot 15		Lot 16	
	Root	Tip	Root	Tip	Root	Tip	Root	Tip
A	1.00	1.00	1.10	1.10	0.60	0.60	0.60	0.60
Y (PPM)	10	18	28	35	9	18	8	15
B	10	18	25	32	15	30	13	25
Al (%)	6.04	6.12	6.17	6.18	--	--	--	--
Si (%)	0.036	0.035	0.069	0.056	0.080	0.071	0.067	0.054
Zr (%)	0.003	0.003	0.002	0.002	--	--	--	--
C	3550	735	--	--	3300	710	--	--

A - Index for Initial Y Content
B - Index for Y Retention Efficiency
C - Metal-Ceramic Contact Time (sec)
* - Average Value

From a geometry point of view, the casting root region has a lower surface to volume ratio than the tip region, thus we would expect the root region to have a higher Y retention efficiency than the tip region. On the other hand, Figure 15 shows that the root region always has a significantly higher isochron than the tip region, indicating the Y content in the root region should be lower than the tip region. Table 1 shows, for all molds, the actual Y content and the retention efficiency in the root region is lower than that of the tip region. These results indicate that the influence of isochron (metal-ceramic contact time) on Y retention efficiency is more important than that of geometry (surface to volume ratio).

Slivers. Slivers (Figure 16) are grains forming streaks in the microstructure. They are usually aligned close to the primary direction, but misoriented in the transverse direction[1]. The formation of slivers is believed to be related to the metal inclusion content during the casting. These inclusions serve as the nuclei for the formation of slivers. A higher inclusion content results in a higher sliver formation tendency. Assuming a constant inclusion content of the input material, the actual inclusion content during the casting depends on the chemical reaction rate between metal and ceramics (mold and core). Thus, casting sliver formation tendency, similar to Y retention efficiency, is predicted by the casting solidus isochron plot. A higher solidus isochron (i.e., higher metal-ceramic contact time) indicates a higher inclusion content and, hence, a higher sliver formation tendency. The isochron of castings of Lot 15 is lower than that of Lot 5 (Figure 15), which indicates that castings of Lot 15 should have fewer slivers than castings of Lots 5 and 11 to 13 (these four molds have the same casting conditions). A similar conclusion is obtained for Lot 16. Grain inspection results of these molds show that castings of Lots 5, and 11 to 13 have 5% slivers, whereas castings of Lots 15 and 16 have none.

Conclusion

Finite-element modeling proves to be an effective tool for understanding the solidification sequence and predicting the microstructures, defects and chemistry variation of investment cast, complex-shaped, single crystal turbine airfoils. Comparison of model predictions to experimental inspection results shows:

1. Both PDAS and SDAS are a function of the LST or the average cooling rate between the alloys liquidus and solidus temperatures. Based on the previously established relationship between DAS and LST, the distribution of casting DAS can be predicted.

2. Primary dendrite growth direction is directly opposite to the heat flow direction and is perpendicular to the mushy zone contour. Thus, the casting isotherm plot (especially the mushy zone contour) can be used to predict various types of grain defects such as LAB, HAB, bigrains and multigrains.

3. The mushy zone contour is also used to predict the magnitude of the angle between the primary dendrite growth direction and the casting stacking axis. This type of defect is called a misoriented dendrite (MOD). The larger the angle of the MOD, the higher the tendency for the casting to be rejected by the Laue' x-ray inspection.

4. Freckles are predicted by the average cooling rate between the alloy's liquidus and solidus temperatures. The casting cooling rate should be higher than a specified value to avoid the formation of freckles.

5. The casting's G/R at liquidus temperature value should be higher than a specified value to avoid the formation of equiaxed grains.

6. Macroshrink is predicted by the contour of the solidus isochron. If there is an isolated spot where the time to reach the solidus temperature is higher than the surrounding area (i.e. metal in the spot is the last to solidify), macroshrink forms in that area.

7. Microporosity (both surface and internal) is controlled by the value of G/R at the solidus temperature. The lower the G/R value, the higher the tendency for microporosity to form.

8. Isochron is also used to predict the formation tendency of sliver grains and the retention efficiency of active elements such as yttrium. Both phenomena are related to the chemical reaction rate between molten metal and ceramics (mold and core) which is then related to the molten metal-ceramics contact time. The higher the metal-ceramic contact time, the lower the Y retention efficiency and the higher the sliver formation tendency.

Acknowledgments

Part of this work (HPTV and LPTB) was supported by contract No. F33615-85-C-5014 (GEAE was the primary contractor and PCC Airfoils was a subcontractor to GEAE) with the Air Force Wright Research and Development Center, Manufacturing Technology Directorate (WRDC/MT), Wright-Patterson AFB. The HPTB portion of the work was sponsored by GEAE (P.O. No. 200-14-10W95668).

References

1. K.O. Yu et al.; "Solidification Modeling of Single Crystal Investment Casting", AFS Transactions, 1990, 417-428.

2. R. Mehrabian; Proceedings of the Int. Conf. on Rapid Solidification Processing, (Reston, VA, 13-16 Nov 1977), 9-27.

3. M. Cohen, B.H. Kear and R. Mehrabian; Proc. 2nd Int. Conf. on Rapid Solidification Processing, (Reston, VA, Mar 1980), 1-23.

4. M. McLean; Directionally Solidified Materials for High Temperature Service, (The Metals Society, London, 1983).

5. M.C. Flemings and G.E. Nereo; "Trans. Met. Soc.", AIME, 239 (1967), 1449-1461.

6. M.C. Flemings, R. Mehrabian and G.E. Nereo; "Trans. Met. Soc.", AIME, 242 (1968), 41-49.

7. S. Lou, D.R. Poirier, and M.C. Flemings; "Met. Trans. B.", 9B, (1978), 771.

8. J.A. Domingue, K.O. Yu and H.D. Flanders; Characteristics of Macrosegregation in ESR IN-718, (Symposium of Fundamentals of Alloy Solidification Applied to Industrial Processes, NASA, Cleveland, OH, Sep 1984), 139-149.

9. M. Gell and D.N. Duhl; Processing and Properties of Advanced High Temperature Alloys, S. Allen et al. editors, (Metals Park, OH: ASM, 1986), 41.

10. M.J. Beffel, K.O. Yu, M. Robinson and K.R. Schneider; "Computer Simulation of Investment Casting Processes", JOM, 41, (2) (Feb 1989), 27-30.

11. L. Quichou, F. Lavand and G. Lesoult; Superalloys 1980, Proc. of the 4th Int. Symp. on Superalloys, J.K. Tien et al. editors, (Metals Park, OH: ASM, 1980), 205.

12. E. Niyama, T. Uchida, M. Morikawa and S. Saito; CIATF, Paper No. 10 (1982).

13. J. Lecompte-Beckers; "Study of Microporosity Formation in Nickel-Base Superalloys", Met. Trans. A, 19A (Sep 1988), 2341-2348.